Article

Theoretical Verification of Photoelectrochemical Water Oxidation Using Nanocrystalline TiO$_2$ Electrodes

Shozo Yanagida [1,*], Susumu Yanagisawa [2,†], Koichi Yamashita [3], Ryota Jono [3] and Hiroshi Segawa [4,†]

[1] Frontier Research Institute, Osaka University, 2-1, Yamada-oka, Suita, Osaka 565-0871, Japan

[2] Department of Physics and Earth Sciences, Faculty of Science, University of the Ryukyus, 1, Senbaru, Nishihara, Okinawa 903-0213, Japan; E-Mail: shou@sci.u-ryukyu.ac.jp

[3] Department of Chemical System Engineering, School of Engineering, The University of Tokyo, 7-3-1 Hongo, Bunkyo-ku, Tokyo 113-8656, Japan; E-Mails: yamasita@chemsys.t.u-tokyo.ac.jp (K.Y.); jono@tcl.t.u-tokyo.ac.jp (R.J.)

[4] Research Center for Advance Science and Technology, The university of Tokyo, 4-6-1, Komaba, Meguro-ku, Tokyo 153-8904, Japan; E-Mail: csegawa@mail.ecc.u-tokyo.ac.jp

† The authors contributed equally to this work.

* Author to whom correspondence should be addressed; E-Mail: yanagida@mls.eng.osaka-u.ac.jp; Tel.: +81-90-1073-9244; Fax: +81-72-792-1914.

Academic Editor: Pierre Pichat

Abstract: Mesoscopic anatase nanocrystalline TiO$_2$ (nc-TiO$_2$) electrodes play effective and efficient catalytic roles in photoelectrochemical (PEC) H$_2$O oxidation under short circuit energy gap excitation conditions. Interfacial molecular orbital structures of (H$_2$O)$_3$ &OH(TiO$_2$)$_9$H as a stationary model under neutral conditions and the radical-cation model of [(H$_2$O)$_3$&OH(TiO$_2$)$_9$H]$^+$ as a working nc-TiO$_2$ model are simulated employing a cluster model OH(TiO$_2$)$_9$H (Yamashita/Jono's model) and a H$_2$O cluster model of (H$_2$O)$_3$ to examine excellent H$_2$O oxidation on nc-TiO$_2$ electrodes in PEC cells. The stationary model, (H$_2$O)$_3$&OH(TiO$_2$)$_9$H reveals that the model surface provides catalytic H$_2$O binding sites through hydrogen bonding, van der Waals and Coulombic interactions. The working model, [(H$_2$O)$_3$&OH(TiO$_2$)$_9$H]$^+$ discloses to have a very narrow energy gap (0.3 eV) between HOMO and LUMO potentials, proving that PEC nc-TiO$_2$ electrodes become conductive at photo-irradiated working conditions. DFT-simulation of stepwise oxidation of a hydroxide ion cluster model of OH$^-$(H$_2$O)$_3$, proves that successive two-electron

oxidation leads to hydroxyl radical clusters, which should give hydrogen peroxide as a precursor of oxygen molecules. Under working bias conditions of PEC cells, nc-TiO$_2$ electrodes are now verified to become conductive by energy gap photo-excitation and the electrode surface provides powerful oxidizing sites for successive H$_2$O oxidation to oxygen via hydrogen peroxide.

Keywords: DFT; HOMO; LUMO; spin density; conductivity; TiO$_2$ photocatalysis; DSC; Honda/Fujishima effect

1. Introduction

Photoelectrochemical (PEC) water (H$_2$O) oxidation on TiO$_2$ electrodes was qualitatively explained as due to downward band bending induced by depletion layer of TiO$_2$ rutile crystal electrodes by assuming the energy structure of TiO$_2$, e.g., conduction band potential (E$_{cb}$) of −0.65 V(SCE) and valence band potential (E$_{vb}$) of 2.35 V (SCE), energy gap 3.0 eV, and 1.23 eV of the equilibrium cell potential for H$_2$O electrolysis at 25 °C and 1 atmospheric pressure [1,2]. We noticed recently that efficient photoelectrochemical H$_2$O oxidation using anatase nc-TiO$_2$ electrodes was at first reported in 1987 by Sakka *et al*. [3]. Interestingly, they reported vigorous oxygen (O$_2$) and hydrogen (H$_2$) evolution using acidic aqueous solution (0.1 N H$_2$SO$_4$) at the PEC nc-TiO$_2$ cell. It is worth noting that the notable electron flow due to H$_2$O oxidation to O$_2$ becomes detectable when bias potential reaches at about 2.0 V (*vs*. SCE), and that under energy gap UV irradiation, photocurrent starts to flow at bias potential around −0.5~−0.3 V (*vs*. SCE), showing vigorous O$_2$ and H$_2$ evolution at bias potential around 0.5–1.0 V (*vs*. SCE). Such effective acidic H$_2$O oxidation on mesoporous nc-TiO$_2$ electrodes prompts us to understand the H$_2$O photooxidation on the basis of molecular orbital (MO) theory, because the band-bending concept is based on crystal-level physics, and nc-TiO$_2$ in PEC electrodes is too small to form depletion layer in nc-TiO$_2$ with average size of 25 nm.

Computational chemistry using density functional theory (DFT) well explains and predicts molecular energy structures and properties functioned by self-association of molecules where hydrogen bonding or van der Waals and Coulombic interactions as non-covalent bonding play an essential role [4–9]. DFT calculations using the nc-TiO$_2$ model of Ti$_9$O$_{18}$H-OH (Yamashita/Jono model) successfully verified that the surface complex between nc-TiO$_2$ and 7,7,8,8-tetracyanoquinodimenthane shows charge transfer transition [10]. We now report verification of PEC oxidation of H$_2$O on nc-TiO$_2$ electrodes on the basis of DFT simulation using Yamashita/Jono nc-TiO$_2$ model. Here, DFT-simulations verify that H$_2$O forms H$_2$O clusters via hydrogen bonding and that the H$_2$O clusters-associated nc-TiO$_2$ electrodes provide excellent H$_2$O oxidation sites. In addition, the working models of H$_2$O clusters-associated PEC-nc-TiO$_2$ electrodes are simulated as radical cations, and effective PEC H$_2$O oxidation is verified as well theoretically.

2. Results and Discussion

2.1. Yamashita/Jono Model for Simulation of PEC-nc-TiO₂ Electrodes

Yamashita and Jono's anatase nc-TiO₂ model ($Ti_9O_{18}H$-OH) consists of nine TiO₂ units $(TiO_2)_9$ derived from the packing unit of the crystalline anatase TiO₂, hydroxide on surface side of the TiO₂ and hydrogen on one side of the TiO₂. To optimize the non-covalent distance between hydroxyl group and nc-TiO₂ unit, all heavy atoms of the nc-TiO₂ unit are frozen and the model was simulated to the energetically optimized geometry (see Supplementary Figure S1). The distance (1.862 Å) become shorter, and the refined Yamashita/Jono model is abbreviated as $OH(TiO_2)_9H$ hereafter and size of about 1 nm length, Mulliken charge, the energy structures and configurations of the highest occupied molecular orbital (HOMO) and the lowest unoccupied molecular orbital (LUMO) are shown in Figure 1.
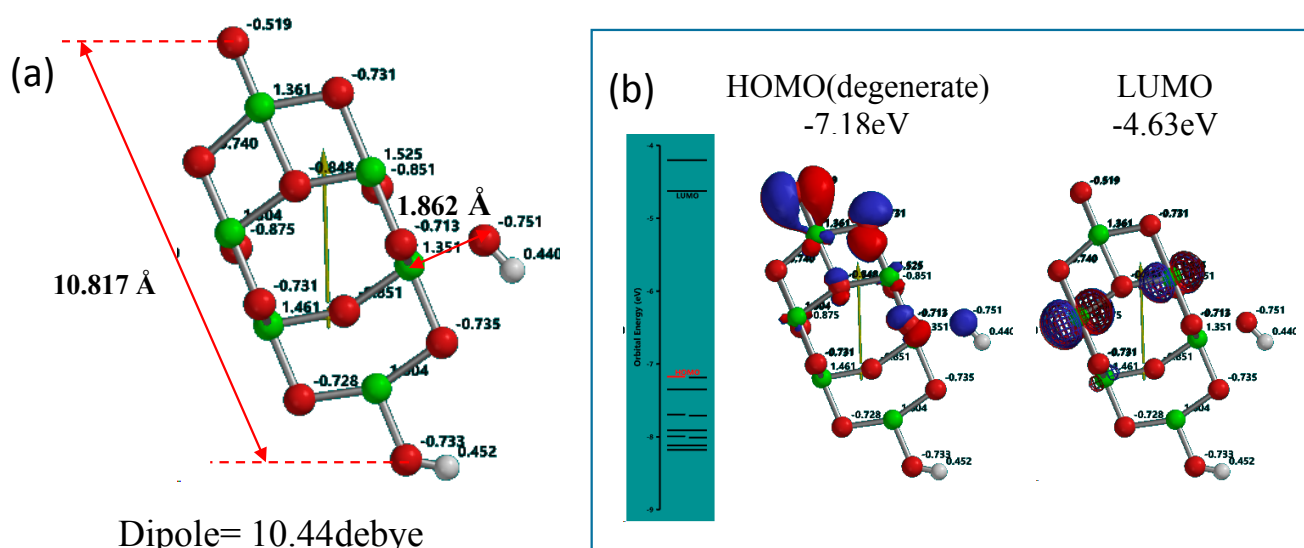
Figure 1. Yamashita/Jono model of $OH(TiO_2)_9H$ as a model of PEC-nc-TiO₂ electrodes, (**a**) Size, distance and Mulliken charge; (**b**) the energy structure and configuration of HOMO and LUMO.

Mulliken charge in $OH(TiO_2)_9H$ indicates that hydroxyl group is charged negative and the protonated nc-TiO₂ unit positive, and then we regard that Yamashita/Jono model is a kind of ion-dipole complex or weak charge transfer complex. The HOMO distributes exclusively on hydroxide ion and the LUMO inside of the nc-TiO₂ unit, giving energy gap 2.55 eV. To know self-association of Yamashita/Jono model, the OH and H-detached $(TiO_2)_9$ and $(TiO_2)_9H$ units are both DFT-simulated as charge is neutral and cation, respectively (Supplementary Tables S1 and S2 and Figures S1 and S2).

The DFT simulation data reveals that Mulliken charge on the hydrogen-bearing side is positive and another side negative as well as the $OH(TiO_2)_9H$ model. Further, the HOMO and LUMO are almost degenerate. The association through van der Waals and Coulombic interaction and the comparable dipole to that of the Yamashita/Jono model support that Yamashita/Jono model may self-associate with $(TiO_2)_9$ and $(TiO_2)_9H$ to yield surface thin-film anatase TiO₂ electrodes as depicted in Figure 2.
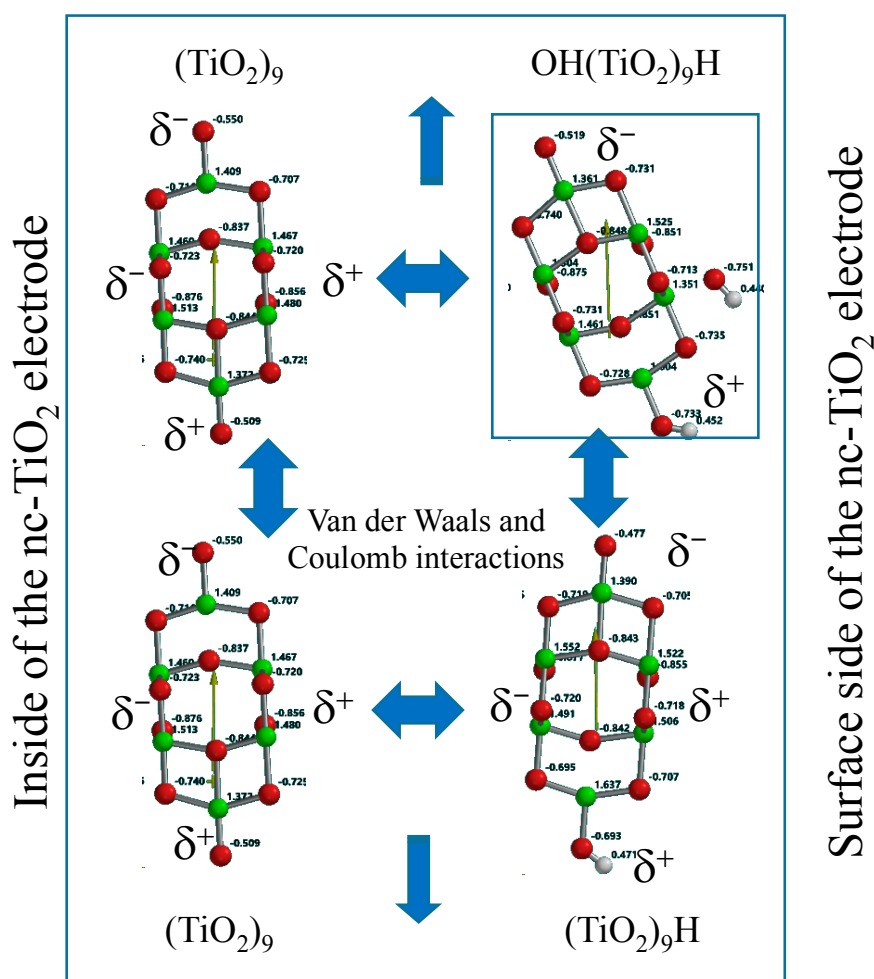
Figure 2. Association of Yamashita/Jono model via van der Waals and Coulomb interactions, explaining growth of the model to larger size PEC-nc-TiO₂ electrodes

2.2. Water Cluster Models for Modeling of Interface Structures of PEC-nc-TiO₂ Electrodes

Water (H_2O) molecules aggregate each other via hydrogen bonding. The structures of H_2O clusters $(H_2O)_n$ (n = 1~3, 6) are simulated to understand their molecular orbital energy structures (Supplementary Table S3). One of the $(H_2O)_3$ trimer is simulated to have dipole and the highest HOMO potential −6.67 eV. The HOMO distributes on the H_2O, of which hydrogen atoms have hydrogen bond with oxygen atoms of other two H_2O, rationalizing the most positive HOMO potential among the examined H_2O clusters. In other words, the trimer $(H_2O)_3$ is the most oxidizable H_2O model.

Similarly, H_2O hydroxide ion clusters and H_2O hydronium ion clusters are simulated (Supplementary Tables S4 and S5). In general, H_2O hydroxide ion clusters have positive HOMO potential. With increase of H_2O molecules, the HOMO shifts to negative potential, which means that HOMO potential is controllable by number of associating H_2O as pH is controllable by dilution. In addition, all of H_2O hydronium ion clusters have very negative HOMO potential −20.2~−12.36 eV with large size of LUMO configurations (Supplementary Table S5). With increase of H_2O molecules, HOMO potential shifts to positive potential, verifying that the HOMO level is changeable as is the case of H_2O hydroxide ion clusters, and the hydrated hydronium ion clusters become oxidizable energetically.

With these simulations and considerations, the polar $(H_2O)_3$ and $OH^-(H_2O)_3$ are employed for DFT-modeling of neutral interface of PEC-nc-TiO$_2$ electrodes. As for hydronium ion cluster, $H_3O^+(H_2O)_2$, which is derived from $(H_2O)_3$, are introduced for the modeling of acidic interface of PEC-nc-TiO$_2$ electrodes (Figure 3). The HOMO configurations indicate that the model clusters have electron rich parts with a wide variety of potentials ranging from −1.07 to −13.5 eV.
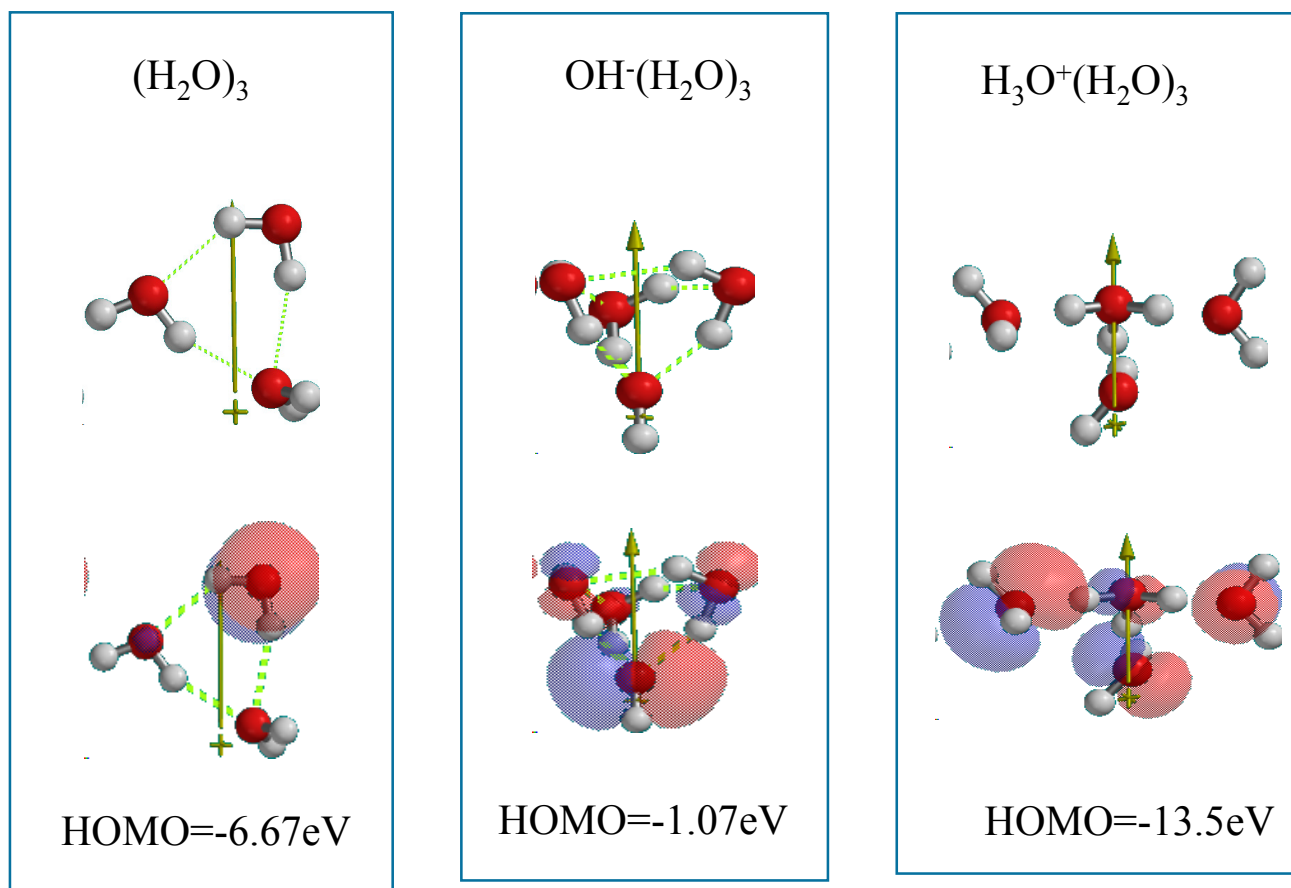
Figure 3. Water cluster models for DFT simulation of PEC oxidation of water molecules on PEC-nc-TiO$_2$ electrodes.

2.3. Photoelectrochemical Oxidation of H$_2$O on PEC-nc-TiO$_2$

As an interface model of nc-TiO$_2$ electrodes, the Yamashita/Jono model, OH(TiO$_2$)$_9$H, is structurally frozen and three H$_2$O molecules are made manually to interact via hydrogen bonding with the frozen hydroxyl group in Yamashita/Jono model. The $(H_2O)_3$-hydrogen bonded model structure is optimized by molecular mechanics (MMFF operation in Spartan), and the molecular orbital is verified by DFT-single-point simulation of an interface structure of $(H_2O)_3$&OH(TiO$_2$)$_9$H as a stationary model (Figure 4). Mulliken charge and electrostatic potential map indicates that negative charge locates on surface oxygen atoms of TiO$_2$ and of the $(H_2O)_3$ cluster, and the more negative charge (stronger red color) on the H$_2$O molecule in the cluster is worth noting in the stationary state model structure.

In the stationary model, configurations of HOMO distributes on one H$_2$O of the cluster $(H_2O)_3$ unit, and LUMO inside the nc-TiO$_2$ unit. Interestingly, the energy gap (0.73 eV) between HOMO and LUMO is smaller than the energy gap (2.55 eV) in the stationary state of Yamashita/Jono model. This

fact suggests that nc-TiO₂ surface binds H₂O molecules via hydrogen bond, forming kinds of charge transfer complexes. In addition, HOMO(−1) (−7.4 eV) distributes on the whole $(H_2O)_3$ unit, implying more effective H_2O oxidation under negative potential of −7.4 eV (Figure 4).

For comparison, only one H_2O-associated Yamashita/Jono model, $H_2O\&OH(TiO_2)_9H$, is simulated as the simplest structure of PEC-nc-TiO₂ electrodes (Supplementary Figure S3). The energy gap (1.75 eV) is given and the hydrogen-bonded H_2O molecule locates HOMO(−1) at −7.8 eV. The simplest orbital energy structure verifies that nc-TiO₂ electrodes intrinsically work as catalytic sites of H_2O oxidation through hydrogen bonding with H_2O molecules.

Figure 4. DFT-simulation of $(H_2O)_3\&OH(TiO_2)_9H$ as a stationary state of PEC-nc-TiO₂ electrodes, (**a**) Mulliken charge and electrostatic density map; (**b**) energy structures of HOMO and LUMO; (**c**) the configuration of HOMO(−1) on $(H_2O)_3$.

When nc-TiO₂ electrodes are energy-filled by UV-irradiation at short circuit PEC conditions, photoelectron on nc-TiO₂ is ejected to conducting grids instantly, and photocurrent become observable. The $(H_2O)_3$-associated PEC-nc-TiO₂ model is simulated as radical cation model of $[(H_2O)_3\&OH(TiO_2)_9H]^+$ as the energy-filled structure under working conditions (Figure 5). Interestingly, the radical cation model as the working model is endothermically simulated ($\Delta E = 192.85$ kcal/mol). The orbital energy analysis of the energy-filled model of $[(H_2O)_3\&OH(TiO_2)_9H]^+$ reveals that the energy gap between HOMO and LUMO potential becomes narrow as small as 0.3 eV with largely negative HOMO (−10.2 eV) and LUMO (−9.9 eV) potential. The HOMO and LUMO distribute in the model

with almost the same configurations, and that the spin (unpaired electron) density distributes with the same configuration as the HOMO and LUMO.

The orbital energy analysis of the energy-filled Yamashita/Jono model of $[OH(TiO_2)_9H]^{.+}$ reveals that the energy gap is pretty narrow (0.7 eV) (Supplementary Table S2). These facts suggest that self-organization of Yamashita/Jono model will give photoconductive nc-TiO$_2$ electrodes when the PEC cell is kept at negative oxidation potential at short circuit conditions and energized by band gap excitation. In fact, the sharp rise in photoconductivity of nc-TiO$_2$ electrodes was reported and discussed as an insulator-metal (Mott) transition in a donor band of anatase TiO$_2$ [11]. It is also worth noting that in studies on dye-sensitized nc-TiO$_2$ solar cells (DSC), adsorption of cationic species like tetrabutylammonium cation and sensitizing dye molecules enhanced electron transport in nc-TiO$_2$ electrodes [12,13]. Accordingly, the photo-enhanced electron transport is now verified as a key function of nc-TiO$_2$ electrodes not only in DSC but also in PEC H$_2$O oxidation.
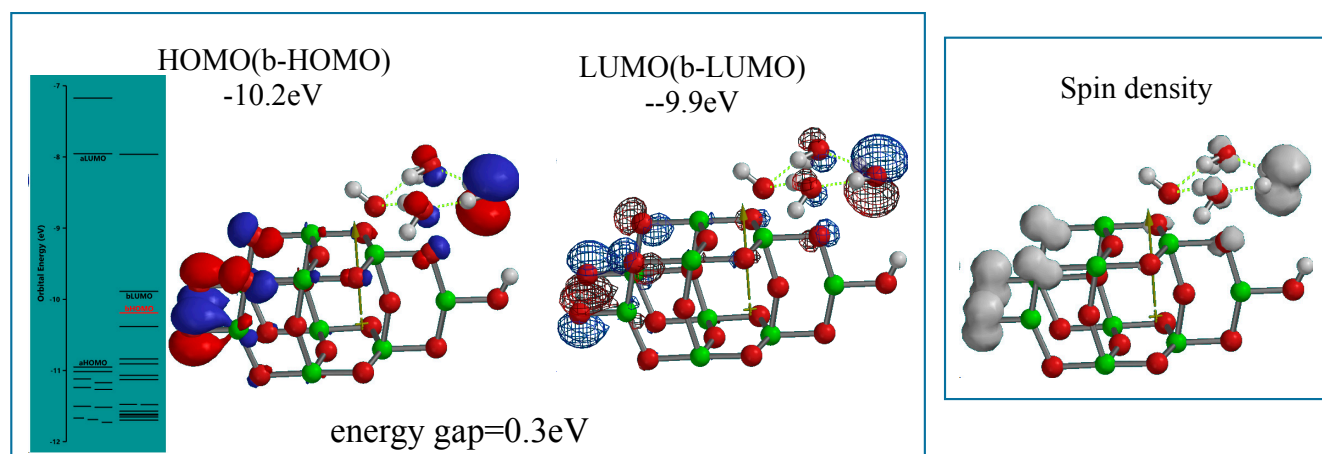
Figure 5. Energy structures of $(H_2O)_3\&[OH(TiO_2)_9H]^+$ as a radical cation model of $(H_2O)_3$-interacted PEC-nc-TiO$_2$ electrode under UV-irradiated bias conditions of PEC-nc-TiO$_2$ electrodes, *i.e.*, a photo-energy-driven operational state model.

The HOMO configuration on the H$_2$O unit at the stationary state of the model, and the spin density distribution on the $(H_2O)_3$ unit at the energy-filled working state strongly suggest that PEC-nc-TiO$_2$ electrodes provides catalytic binding sites of H$_2$O. The same functions of PEC nc-TiO$_2$ electrodes are confirmed by the molecular orbital simulation of the energy-filled $[H_2O\&OH(TiO_2)_9H]^+$ model (Tables S1 and S2, Figure S4). The narrowed energy gap (0.3 eV), the comparable configurations of HOMO, LUMO and spin density are quite comparable with those of $[(H_2O)_3\&OH(TiO_2)_9H]^+$.

2.4. DFT Simulation of H$_2$O Oxidation to Hydrogen Peroxide

In PEC H$_2$O oxidation on nc-TiO$_2$ electrodes, bias potential is essential to start H$_2$O oxidation. The HOMO potential of Yamashita/Jono model, −7.18 eV and the average HOMO potential of H$_2$O clusters, −7.48 eV (Supplementary Table S3) verify that the bias potential >0.3V is at lease required for PEC H$_2$O oxidation under neutral working conditions. On the other hand, the HOMO potential (−10.2 eV) of the working model of $[(H_2O)_3\&OH(TiO_2)_9H]^+$ predicts that successive oxidation should

occur under more negative bias potential (>2.72 eV) for H_2O oxidation to oxygen through formation of hydrogen peroxide.

In order to verify whether hydroxyl radical may form successively on PEC-nc-TiO_2 electrodes, the two-electron oxidation structure of $[H_2O\&OH(TiO_2)_9H]^{..++}$ is simulated as dication-diradical model as another working interface model of PEC-nc-TiO_2 electrodes. The more energy-filled model is endothermically (ΔE = 458.43 kcal/mol) simulated as powerful working model (Figure 6). The energy gap (0.3 eV) and the configuration of HOMO and LUMO are confirmed to verify that such largely energized PEC-nc-TiO_2 electrodes keep photoconductivity with keeping high oxidation potential. The spin density distributes on the $(H_2O)_3$ unit, suggesting that two-electron H_2O oxidation occurs successively on the catalytic site on nc-TiO_2 electrodes.
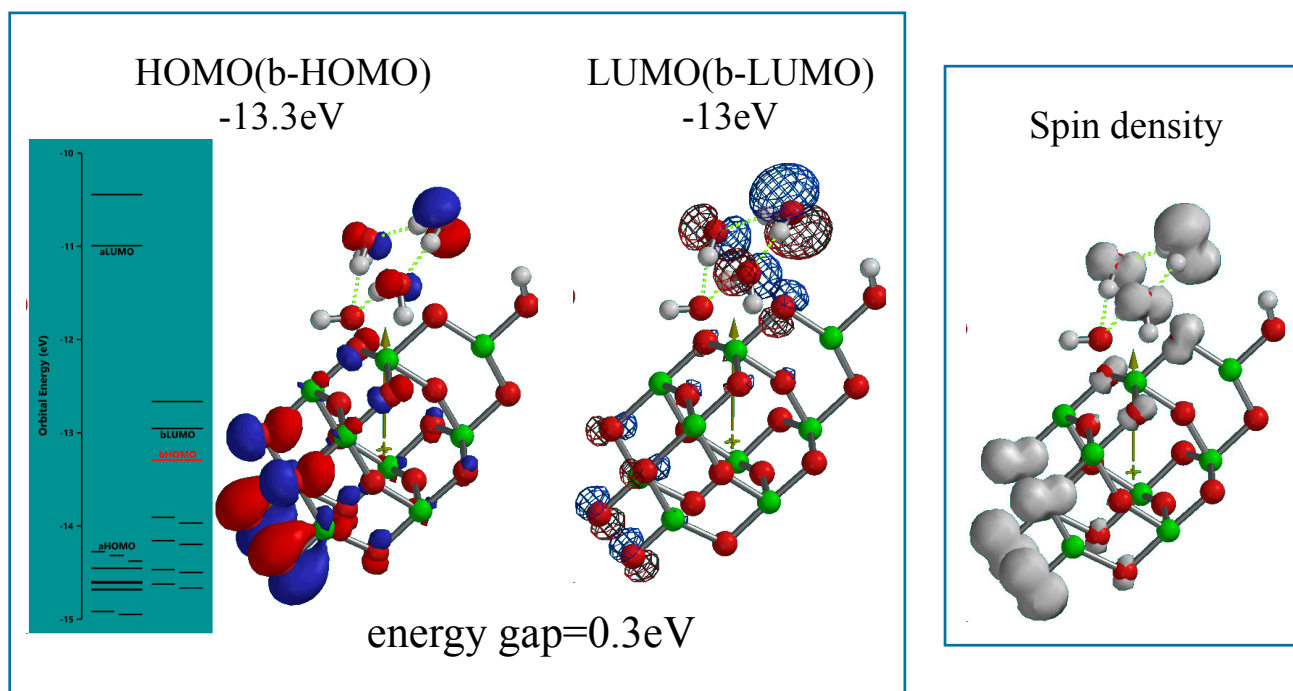
Figure 6. Energy structures of $[(H_2O)_3]\&OH(TiO_2)_9H]^{..++}$ as the model of two electron oxidation state of PEC-nc-TiO_2 electrodes, *i.e.*, the diradical-dication state of the electrodes.

With these simulation analyses, step-wise PEC-H_2O oxidation is shown in Scheme 1. One-electron oxidation of H_2O molecule yields radical cation of H_2O (H_2O^+) and the removable of proton from the radical cation (deprotonation) leads to hydroxyl radical (HO) (Equations (1) and (2) in Scheme 1). When H_2O hydroxide ion cluster of $OH^-(H_2O)_3$ undergoes further oxidation, another hydroxyl radical favorably forms in neighbor on PEC-nc-TiO_2 electrodes, and efficient and effective formation of hydrogen peroxide occurs (Equation (3) in Scheme 1).

$$H_2O \xrightarrow{-e} [H_2O]^{\cdot+} \xrightarrow{-H^+} HO^{\cdot} \dashrightarrow (1)$$

$$OH^-(H_2O)_3 \xrightarrow{-e} \left[[OH^-(H_2O)_3]^{\cdot+} \rightleftharpoons [OH^{\cdot}(H_2O)_3] \right] \dashrightarrow (2)$$

$$OH^-(H_2O)_3 \xrightarrow{-2e} \left[[OH^-(H_2O)_3]^{\cdot\cdot++} \rightleftharpoons [(OH^{\cdot})_2(H_2O)_2H]^+ \right] \xrightarrow{-(H_2O)_2H^+} HOOH \dashrightarrow (3)$$
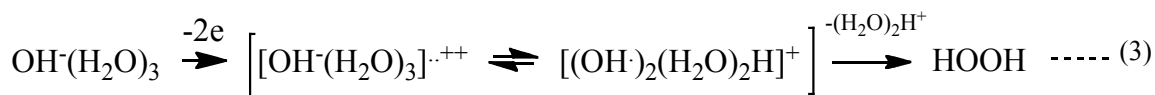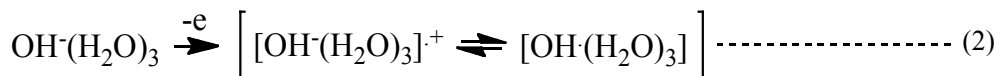
Scheme 1. PEC-H_2O oxidation to hydrogen peroxide as a precursor of oxygen molecule.

Figure 7 shows DFT-simulation results of oxidation of $OH^-(H_2O)_3$ to $[OH^-(H_2O)_3]^{\cdot+}$ or $[OH^{\cdot}(H_2O)_3]$ as one-electron oxidation products (Equation (2)), and to $[OH^-(H_2O)_3]^{\cdot\cdot++}$ or $[(OH^{\cdot})_2(H_2O)_2H]^+$ as two-electron oxidation products. They are simulated endothermically, suggesting that they are in energy filled states (Supplementary Table S6). In the equilibrium geometry of $[OH^{\cdot}(H_2O)_3]^{\cdot+}$, the spin density distributes only on the hydroxyl group, and the Mulliken charge on hydroxyl group decreases largely from −0.900 to −0.404. Thus the one-electron oxidation product has the structure of $[OH^{\cdot}(H_2O)_3]$ rather than $[OH^-(H_2O)_3]^{\cdot+}$.
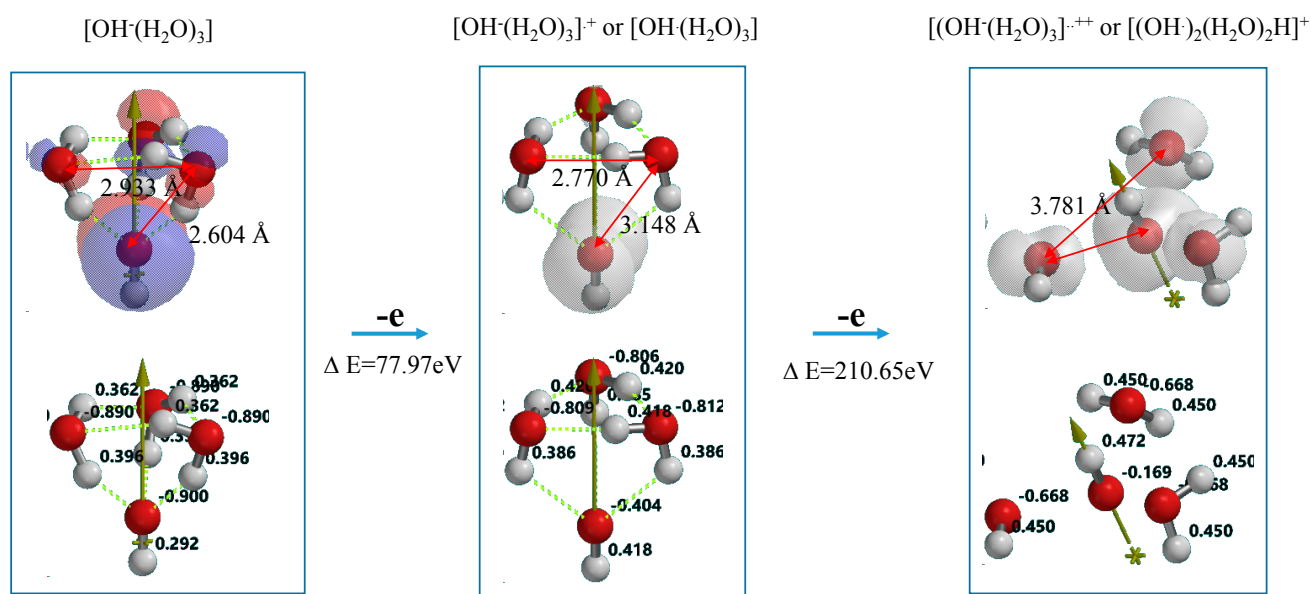
Figure 7. DFT-simulation of step-wise oxidation of the hydroxide ion cluster model of $[OH^-(H_2O)_3]$

On the other hand, the two-electron oxidation product shows that the spin density distributes on hydroxyl group and the $(H_2O)_3$ units. The Mulliken charge on them decreases from −0.806 to −0.668. The distance between hydroxyl group and H_2O is shortened from 3.148 Å to 2.239 Å and the hydrogen bonds observed in $[OH^-(H_2O)_3]^{\cdot+}$ disappear. In addition, the hydrogen-oxygen bond distance of H_2O (0.976 Å) in $[OH^-(H_2O)_3]^{\cdot\cdot++}$ is quite comparable with that (0.988 Å) in $[OH^-(H_2O)_3]^+$. The H_2O components in the most energy-filled cluster $[OH^-(H_2O)_3]^{\cdot\cdot++}$ should be tightly aggregated one another. Detachment of $(H_2O)_3H^+$ from $[(OH^{\cdot})_2(H_2O)_2H^+]$ leaves two hydroxyl radical in neighbor, yielding hydrogen peroxide as a precursor of O_2 molecule (Equation (3) in Scheme 1). The oxidation of neutral

H_2O is verified to occur initially in photocatalytic processes to give effectively hydrogen peroxide on PEC nc-TiO_2 electrodes.

2.5. Verification of the Sakka's PEC H₂O Oxidation under Acidic Conditions

The stationary model of $H_3O^+(H_2O)$-associated structure of $H_3O^+(H_2O)\&OH(TiO_2)_9H$ and two kinds of energy filled models, $[H_3O^+(H_2O)\&OH(TiO_2)_9H]^{\cdot+}$ and $[H_3O^+(H_2O)\&OH(TiO_2)_9H]^{\cdot\cdot++}$ are simulated as an interface model of PEC-nc-TiO_2 electrodes under Sakka's acidic conditions (Supplementary Figures S5 and S6). However, the energy gap are rather wider and the spin density does not localize on $H_3O^+(H_2O)$ in the most energized state of $[H_3O^+(H_2O)\&OH(TiO_2)_9H]^{\cdot\cdot++}$.

The hydronium ion cluster, $H_3O^+(H_2O)_2$ represent less acidic than $H_3O^+(H_2O)$ (Supplementary Table S5). The stationary states of $H_3O^+(H_2O)_2$-associated structure of $H_3O^+(H_2O)_2\&OH(TiO_2)_9H$ is simulated as an interface model under Sakka's less acidic conditions, and analyzed as well in view of molecular orbital energy structure (Figure 8).
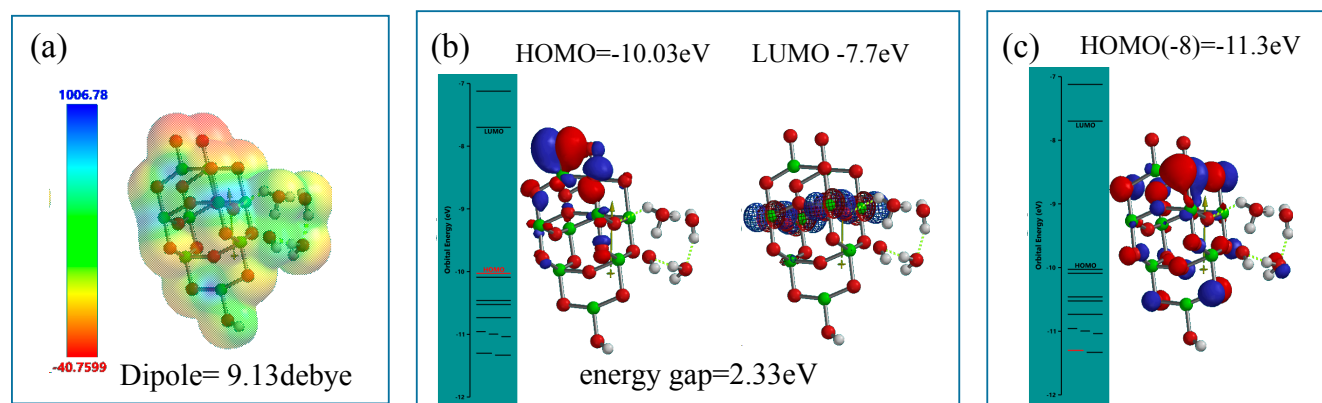
Figure 8. DFT-simulation of $H_3O^+(H_2O)_2\&OH(TiO_2)_9H$ as a model of hydronium ion clusters on PEC-nc-TiO_2 electrodes, (**a**) electrostatic potential map; (**b**) structures of HOMO and LUMO; (**c**) Configuration of HOMO(−8).

Differently from the modeling for the neutral PEC H_2O oxidation, electrostatic potential map indicates that negative charge locates much more on the nc-TiO_2 unit rather than the H_2O unit, and HOMO distributes only on oxygen atoms in the nc-TiO_2 unit. The energy gap 2.33 eV implies weak association of acidic H_2O on nc-TiO_2 electrodes. The orbital energy indicates that HOMO(−8) distributes slightly on the $H_3O^+(H_2O)_2$ unit with very negative potential of −11.3 eV.

The acidic interface model of $[H_3O^+(H_2O)_2\&OH(TiO_2)_9H]$ is simulated to $[H_3O^+(H_2O)_2\&OH(TiO2)_9H]^{\cdot+}$ as the radical cation of the one-electron oxidation state, and to $[H_3O^+(H_2O)_2\&OH(TiO2)_9H]^{\cdot\cdot++}$ as the diradical-dication model of the two electron oxidation sate (Figure 9). The former radical cation model reveals that configurations of HOMO, LUMO and spin density distribute on the nc-TiO_2 unit and not on the $H_3O^+(H_2O)_2$, and the energy gap 0.7eV is not favorable in view of photoconductivity compared to that under neutral conditions. However, HOMO(−1) distributes on the $(H_2O)_2$ unit with orbital potential of −13.9 eV.
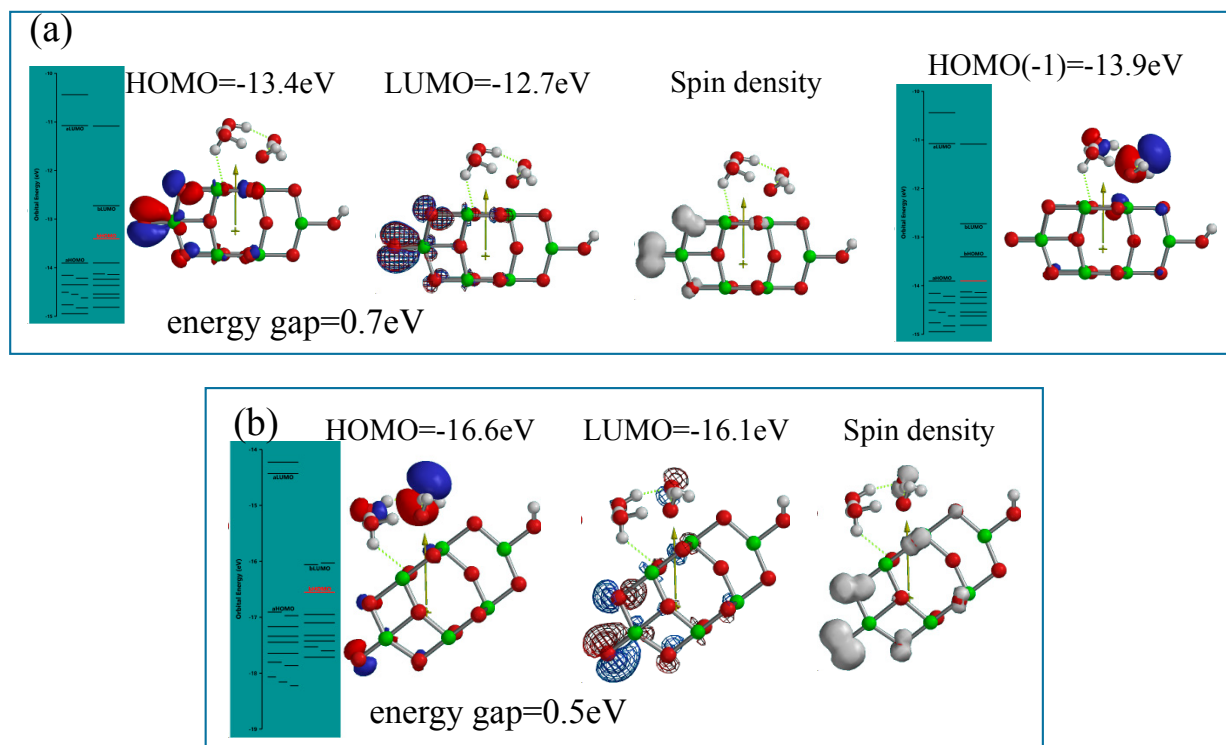
Figure 9. DFT-simulation of oxidation states of $H_3O^+(H_2O)_2\&OH(TiO_2)_9H$, (**a**) energy structures of the one-electron oxidation state, $[H_3O^+(H_2O)_2\&OH(TiO_2)_9H]^{\cdot+}$; (**b**) energy structures of the two-electron oxidation state, $[H_3O^+(H_2O)_2\&OH(TiO_2)_9H]^{\cdot\cdot++}$.

As for the latter dication-diradical model, the energy gap 0.5 eV and HOMO potential, -16.6 eV are given, and the spin density distributes on $H_3O^+(H_2O)_2$ unit. Accordingly, the DFT-based orbital energy structure verifies that PEC H_2O oxidation occurs even under acidic conditions, when nc-TiO_2 electrodes are energized by bias potential under energy-gap UV irradiation.

3. Experimental Section

DFT calculations were performed using the B3LYP exchange-correlation functional and the 6-31G(d) basis set with *Spartan'14* (Wavefunction, Inc. Irvine, CA, USA) installed on VAIO Model SVP132A1CN, Intel(R) core(TM)i7-4500U CPU and on VAIO PC-Z (Intel core 2 Duo processor T9900, system memory (RAM) 8G and hard disk drive, SSD 128, 2GB).

Molecular mechanic optimization (e.g., Merck Molecular Force Factor (MMFF) operation in Spartan program) and DFT (B3LYP 6-31G*) modeling determine molecular orbital structure of equilibrium geometry as an inter-atomic potential model [7,8]. In the case of Spartan program, molecular orbital energy structures (HOMO(0~9), LUMO(0~1)), their configurations, electrostatic potential map, spin (unpaired electron of radical) density are visualized by graphic conveniently.

As for interface energy-filled model structures with unpaired electron, *i.e.*, radical cations, orbital energy diagrams are shown in two ways, affixed 'a-' and 'b-' because the radical cations have two available wave functions. The 'b'-HOMO and 'b'-LUMO are employed, since 'β'-HOMO configurations are almost the same as spin density configurations. Electron energy gap of the radical cation components is obtained from energy difference between 'b'-HOMO and 'b'-LUMO. Mulliken charge,

spin densities and their maps are informative for theoretical understandings of energy structures of energy-filled molecular orbitals of nc-TiO$_2$ interfaces.

The anatase nc-TiO$_2$ model structure has a pretty large size of OH(Ti$_9$O$_{18}$)H and is named as Yamashita/Jono model. The nc-TiO$_2$ model structure is refined as described in Figure S7. As for orbital configurations, HOMO is shown by solid or solid transparent, LUMO by mesh, and spin density by white solid or white solid transparent. As for color in electrostatic potential map, red is negative, green neutral and blue positive qualitatively. Formation energy (ΔE) of key model molecules is determined from total energy (E) of their related components in Supplementary Tables S1–S3.

4. Conclusions

DFT-based modeling enables to verify molecular orbital level interfacial structures of photo-electrochemically energized nc-TiO$_2$ electrodes. Although nc-TiO$_2$ electrodes are composed of nc-TiO$_2$ particles with average size 25 nm, Yamashita/Jono nc-TiO$_2$ model (length size = ~1 nm) is large enough to model nc-TiO$_2$ electrodes because the model may self-aggregate to larger sizes through hydrogen bond and van der Waals and Coulombic interactions. Water (H$_2$O) cluster models (H$_2$O)$_3$ and H$_3$O$^+$(H$_2$O)$_2$ are appropriate to bind Yamashita/Jono model cluster, providing interfacial PEC-nc-TiO$_2$ electrode structures at neutral and acidic H$_2$O conditions.

Molecular orbital analyses of the stationary and the working PEC-nc-TiO$_2$ cluster models reveal that H$_2$O clusters are adsorbed effectively (catalytically) via hydrogen bonding to PEC-nc-TiO$_2$ electrodes at stationary state, and that the conductivity of PEC-nc-TiO$_2$ electrodes is enhanced without loosing oxidation potential, leading to successive water oxidation to oxygen molecules through hydrogen peroxide in PEC cells. The molecular modeling of nc-TiO$_2$ electrodes in PEC cells verifies that the photo-induced conductivity is the most important driving force of PEC H$_2$O oxidation on nc-TiO$_2$ electrodes. The DFT-verified photoconductivity is true for understanding of photocatalysis of Pt-deposited nc-TiO$_2$ particles and dye-sensitized nc-TiO$_2$ solar cells, rationalizing their remarkable efficiencies and effectiveness.

Supplementary Materials

Supplementary materials can be accessed at: http://www.mdpi.com/1420-3049/20/06/9732/s1.

Author Contributions

Shozo Yanagida, Susumu Yanagisawa, KY, RJ and HS designed research; Shozo Yanagida, Susumu Yanagisawa, KY, RJ and HS performed research, analyzed the data and discussed; Shozo Yanagida, Susumu Yanagisawa wrote the paper. All authors read and approved the final manuscript.

Conflicts of Interest

The authors declare no conflict of interest.

References

1. Grätzel, M. Photoelectrochemical cells. *Nature* **2001**, *414*, 338–344.
2. Hashimoto, K.; Irie, H.; Fujishima, A. Photoelectrochemical cells. *JSAP Int.* **2006**, *24*, 4–20.
3. Yoko, T.; Kamiya, K.; Sakka, S. Photoelectrochemical Properties of TiO_2 Films Prepared by the Sol-Gel Method. *Yogyo Kyoukai-Shi* **1987**, *95*, 150–155.
4. Kanemoto, M.; Hosokawa, H.; Wada, Y.; Murakoshi, K.; Yanagida, S.; Sakata, T.; Mori, H.; Ishikawa, M.; Kobayashi, H. Semiconductor photocatalysis. Part 20. Role of surface in the photoreduction of carbon dioxide catalysed by colloidal ZnS nanocrystallites in organic solvent. *J. Chem. Soc. Faraday Trans.* **1996**, *92*, 2401–2411.
5. Manseki, K.; Yu, Y.; Yanagida, S. A phenyl-capped aniline tetramer forZ907/*tert*-butylpyridine-based dye-sensitized solar cells and molecular modelling of the device. *Chem. Commun.* **2013**, *49*, 1416–1418.
6. Yanagisawa, S.; Yasuda, T.; Inagaki, K.; Morikawa, Y.; Manseki, K.; Yanagida, S. Intermolecular Interaction as the Origin of Red Shifts in Absorption Spectra of Zinc-Phthalocyanine from First-Principles. *J. Phys. Chem. A* **2013**, *117*, 11246–11253.
7. Hehre, W.J. Chapter 19. Application of Graphical models in book. In *A Guide to Molecular Mechanics and Quantum Chemical Calculations*; Wavefunction, Inc.: Irvine, CA, USA, 2003; p. 473.
8. Hoffmann, R. The frontier orbital perspective in book SOLID and SURFACES. In *A Chemist's View of Bonding in Extended Structures*; Wiley-VCH Inc.: Toronto, ON, Canada, 1988.
9. Agrawal, S.; English, N.J.; Thampi, K.R.; MacElroy, J.M.D. Perspectives on *ab initio* molecular simulation of excited-state properties of organic dye molecules in dye-sensitised solar cells. *Phys. Chem. Chem. Phys.* **2012**, *14*, 12044–12056.
10. Jono, R.; Fujisawa, J.; Segawa, H.; Yamashita, K. Theoretical Study of the Surface Complex between TiO_2 and TCNQ Showing Interfacial Charge-Transfer Transitions. *J. Phys. Chem. Lett.* **2011**, *2*, 1167–1170.
11. Wahl, A.; Augustynski, J. Charge Carrier Transport in Nanostructured Anatase TiO_2 Films Assisted by the Self-Doping of Nanoparticles. *J. Phys. Chem. B* **1998**, *102*, 7820–7828.
12. Kambe, S.; Nakade, S.; Kitamura, T.; Wada, Y.; Yanagida, S. Influence of the Electrolytes on Electron Transport in Mesoporous TiO_2-Electrolyte Systems. *J. Phys. Chem. B* **2002**, *106*, 2967–2972.
13. Nakade, S.; Saito, Y.; Kubo, W.; Kanzaki, T.; Kitamura, T.; Wada, Y.; Yanagida, S. Enhancement of electron transport in nano-porous TiO_2 electrodes by dye adsorption. *Electrochem. Commun.* **2003**, *5*, 804–808.

Sample Availability: Not available.